

A Global *In Vivo Drosophila* RNAi Screen Identifies a Key Role of Ceramide Phosphoethanolamine for Glial Ensheathment of Axons

Aniket Ghosh^{1,2}, Tina Kling^{1,2}, Nicolas Snaidero^{1,2}, Julio L. Sampaio³, Andrej Shevchenko³, Heribert Gras⁴, Bart Geurten⁴, Martin C. Göpfert⁴, Jörg B. Schulz⁵, Aaron Voigt⁵, Mikael Simons^{1,2*}

1 Max Planck Institute for Experimental Medicine, Göttingen, Germany, **2** Department of Neurology, University of Göttingen, Göttingen, Germany, **3** Max Planck Institute of Molecular Cell Biology and Genetics, Dresden, Germany, **4** Department of Cellular Neurobiology, University of Göttingen, Göttingen, Germany, **5** Department of Neurology, University Medical Center, RWTH Aachen, Aachen, Germany

Abstract

Glia are of vital importance for all complex nervous system. One of the many functions of glia is to insulate and provide trophic and metabolic support to axons. Here, using glial-specific RNAi knockdown in *Drosophila*, we silenced 6930 conserved genes in adult flies to identify essential genes and pathways. Among our screening hits, metabolic processes were highly represented, and genes involved in carbohydrate and lipid metabolic pathways appeared to be essential in glia. One critical pathway identified was *de novo* ceramide synthesis. Glial knockdown of *lace*, a subunit of the serine palmitoyltransferase associated with hereditary sensory and autonomic neuropathies in humans, resulted in ensheathment defects of peripheral nerves in *Drosophila*. A genetic dissection study combined with shotgun high-resolution mass spectrometry of lipids showed that levels of ceramide phosphoethanolamine are crucial for axonal ensheathment by glia. A detailed morphological and functional analysis demonstrated that the depletion of ceramide phosphoethanolamine resulted in axonal defasciculation, slowed spike propagation, and failure of wrapping glia to enwrap peripheral axons. Supplementing sphingosine into the diet rescued the neuropathy in flies. Thus, our RNAi study in *Drosophila* identifies a key role of ceramide phosphoethanolamine in wrapping of axons by glia.

Citation: Ghosh A, Kling T, Snaidero N, Sampaio JL, Shevchenko A, et al. (2013) A Global *In Vivo Drosophila* RNAi Screen Identifies a Key Role of Ceramide Phosphoethanolamine for Glial Ensheathment of Axons. *PLoS Genet* 9(12): e1003980. doi:10.1371/journal.pgen.1003980

Editor: Norbert Perrimon, Harvard Medical School, Howard Hughes Medical Institute, United States of America

Received: July 3, 2013; **Accepted:** October 12, 2013; **Published:** December 12, 2013

Copyright: © 2013 Ghosh et al. This is an open-access article distributed under the terms of the Creative Commons Attribution License, which permits unrestricted use, distribution, and reproduction in any medium, provided the original author and source are credited.

Funding: This work was funded by the "Bundesministerium für Bildung und Forschung" ("Nationales Genomforschungsnetz" (NGFN+): 01GS08137/01GS08137-6a to AV and JBS and "Kompetenznetz Degenerative Demenzen" (KNDD): 01GI0703/01GI1005C to JBS). The work was supported by an ERC Starting Grant (ERC-2007–StG. Grant Agreement number: 204034-2 to MS) and grants from the German Research Foundation (SI 746/9-1; TRR43 to MS and SFB889-C2 to MCG) and from the BMBF (E-Rare) and the Tschira Stiftung. The funders had no role in study design, data collection and analysis, decision to publish, or preparation of the manuscript.

Competing Interests: The authors have declared that no competing interests exist.

* E-mail: msimons@gwdg.de

Introduction

Many of the essential functions of glia such as neurotransmitter metabolism, ion buffering, axon pathfinding, electrical insulation, and trophic support are conserved between vertebrates and invertebrates [1,2]. Among the various tasks that glia perform, the ensheathment of axons is one function that is of high clinical relevance as there are several human diseases in which the ensheathing membrane is broken down. In vertebrates, the electrical insulation is executed by specific glial subtypes, oligodendrocyte and Schwann cells, which enwrap axons with myelin, a multilayered compacted lipid-rich membrane stack [3,4]. Even though *Drosophila* glia do not generate myelin, specialized glia that ensheath individual axons or fascicles are present in flies [1,5].

The vital importance of glia in different organisms was clearly illustrated in cell ablation experiments. For example, when oligodendrocytes are ablated in mice, the animals become severely paralyzed and die prematurely [6,7]. Also in *Drosophila*, where glia constitute a minor cell population [8], genetic ablation of glia induces rapid death of the flies [9]. Whereas the evolutionarily

conserved significance of glia is undisputed, little is known about the vital functions of glia. Here, we aimed at identifying genes in glia that are indispensable for the function of the nervous system.

Results and Discussion

A global *in vivo Drosophila* RNAi screen in glia

In order to identify genes with essential function in glia, we performed a global *in vivo* glial-specific RNAi screening. As we were interested in evolutionary conserved glial functions, we restricted our analysis to all fly genes of which a human ortholog could be identified (as provided by the VDRC) comprising roughly 45% of all protein coding genes in the fly. Therefore, a library of 7881 RNAi lines corresponding to 6930 genes with a putative human ortholog was obtained for the screening [10,11]. The scheme of the screening is presented in (Figure 1A). The expression of shRNA was restricted to glial cells in adult flies by using the pan-glial driver line *repo-GAL4* [12,13] in combination with temperature sensitive (ts) *GAL80^{ts}* under the control of the ubiquitous tubulin promoter (*tub-GAL80^{ts}*) [14]. Crossing of virgin females (*tub-GAL80^{ts}; repo-GAL4*) with 2–3 males from *UAS-shRNA*

Author Summary

Glia are essential for the function of any nervous system. The number of glia correlates with the complexity of the nervous system. Important functions of glia include maintaining ionic homeostasis, supporting neurotransmission, and insulating axons to speed up nerve conduction. The biomedical relevance of glia is highlighted by an increasing number of neurological diseases, in which glia appear to play an essential role, ranging from neuropathies to schizophrenia. Here, we performed a global *in vivo* glial-specific RNAi screen of evolutionary conserved genes in *Drosophila*. With this approach, we identified 736 candidate genes that resulted in lethality or motor deficits when knocked down specifically in glia. One essential pathway identified was ceramide phosphoethanolamine biosynthesis, which was found to be important for wrapping glia to extend their membrane around axons of the peripheral nerve. Our study illustrates that a large-scale screen in *Drosophila*, in combination with morphological analysis is able to dissect the basic mechanism of neuron-glia communication and identify candidate genes in human neuropathies.

fly lines were set at 18°C. three to five days post eclosion; male adult flies from F1 generation were shifted to 29°C to induce shRNA expression. After 10 days, RNAi lines showing lethality or climbing deficits (motor defect) in more than 50% of the flies were counted as primary hits. To evaluate the efficiency of the screening system, we performed a pre-screen with selected RNAi lines targeting genes essential for the viability of any cell type. For example, when *UAS-nejire* RNAi transgenic flies were crossed with *tub-GAL80^{ts}; repo-GAL4* virgin female flies, a drastic reduction in the lifespan was observed (Figure 1B). Primary screening data indicated that 11% of the total 7881 RNAi lines used in the screening, showed lethality and 0.45% were scored for motor defects (Figure 1C). Since the aim of our primary screen was to identify genes that result in lethality or severe motor defects when knocked down in glia, but not in other cells, we compared our hits with datasets that were obtained by using the same RNAi library but in combination with *GMR-GAL4* (Figure S1). With this approach, we identified 736 candidates with possibly essential functions in glia (Table S1).

Next, by using the list of primary hits and their predicted human ortholog, we performed a systematic networking analysis by Bingo online resource [15] to reveal gene ontology (GO) annotated biological processes. Among the 736 primary hits, we detected 306 genes with a possible function in metabolic processes and among those 79 genes with a predicted function in glial carbohydrate and lipid metabolic processes. Major carbohydrate pathways identified are glycolysis, pentose phosphate and polysaccharide metabolic pathways, while phospholipid, fatty acid and steroid metabolic process were amongst the lipid metabolic pathways. Since metabolic functions are of particular interest in mammalian glia [16,17], we decided to analyze these hits further in a secondary screen. For the secondary screening, wandering third instar (L3) larval peripheral nervous system (PNS) was chosen because its organization is less complex than that of the central nervous system (CNS). It is easily accessible and renders possible visualization by light and electron microscopy [18,19]. Moreover, at this stage, the glial migration is complete and the terminally differentiated glia ensheath the afferent and efferent axons of the peripheral nerves [20–22]. Axons in each of the peripheral nerve are enwrapped by the wrapping glia, which in turn are encircled

by two types of surface glia, the perineurial glia and subperineurial glia [18,19]. The rationale of the secondary screening was to identify the essential metabolic pathway for glial ensheathment of axons. To visualize the glial membrane, a membrane tagged GFP (*UAS-mCD8-GFP*) [23] was expressed using *repo-GAL4* and immunolabeling against HRP was performed to highlight the axons. For the secondary screening, the candidates from lipid and carbohydrate pathways were selected based on STRING protein association database [24] (Figure S2). Secondary screening resulted in various phenotypes such as glial swelling, axonal wrapping defect and axonal splitting in the larval PNS (Figure S3A–C, Table S2) but no embryonic lethality was observed. One of the most penetrant alterations of axon-glia morphology was observed after glia-specific knockdown of *lace*, a subunit of the serine palmitoyltransferase.

lace is specifically required in wrapping glia

Serine palmitoyltransferase catalyzes the condensation of serine and palmitoyl-CoA to generate 3-ketosphinganine, the rate-limiting step in *de novo* sphingolipid synthesis [25]. Mutations in the two human subunits of the serine palmitoyltransferase are associated with hereditary sensory and autonomic neuropathy [26]. A common feature of the mutations is the loss of canonical enzyme activity and the generation of toxic lipid intermediates [27]. Glial inhibition of *lace* function (*repo>mCD8-GFP/lace* RNAi) resulted in glial bulging and in an alteration of the axonal packing in all eight pairs of abdominal nerves in all larval PNS examined (n = 15) (Figure 1D). The bulging of glia was localized to focal regions, but appeared randomly along the entire peripheral nerves with diameters ranging from 10 μm to 30 μm. Nerves of *repo-GAL4/+* control flies were straight and packed in bundles with a uniform diameter of 5–8 μm (Figure 1E). In contrast, knockdown of *lace* in neurons did not result in any visible alterations of axonal morphology (Figure 1F). The average cross-section area of the nerve were similar in the knockdown (*elav-GAL4/lace* RNAi) and in the *elav-GAL4/+* control flies (Figure 1G).

Notably, the ensheathment defect was not due to a compromised blood-nerve-barrier (Figure S4) as has for example been observed in null *fray* mutants [28]. In addition, the number of glial cells in the peripheral nerves was comparable to control (Figure 2A,B). It is important to note glial cell death affects neuronal survival and results in embryonic lethality [9]. The absence of embryonic lethality and the comparable glial cell number suggested that glial cell death did not occur at the larval stage after knockdown of *lace*. The expression of *lace* in glia was confirmed by double immunolabeling of *lace⁵* [29] (*LacZ* enhancer trap line) with anti-β-galactosidase and anti-*repo* in L3 larval peripheral nerves (Figure 2C). In addition, by RT-PCR analysis of the fly brain and PNS we identified *lace* transcript in the nervous system of both male and female flies (Figure 2D).

Two independent RNAi lines (Transformant ID 21803 and 110181, VDRC) against *lace* showed identical swelling and wrapping defects. In addition, we also observed in hypomorphic *lace* mutant (*lace²/lace⁵*) axonal defasciculation (Figure 2E), ruling out off-target effects of the RNAi lines. As in the *lace*-RNAi knockdown, the average cross-section area of the nerves was increased in the hypomorphic *lace* mutant animals. The mutant phenotypes appeared to be subtle, which is not surprising as complete loss of *lace* during the development is lethal, while this hypomorphic combination are viable even into adulthood [29]. However, 100% penetrance of the phenotype was observed both for the RNAi knockdown (n = 16) and the hypomorphic mutants (n = 16). Importantly, the *lace* mutant phenotype was rescued by

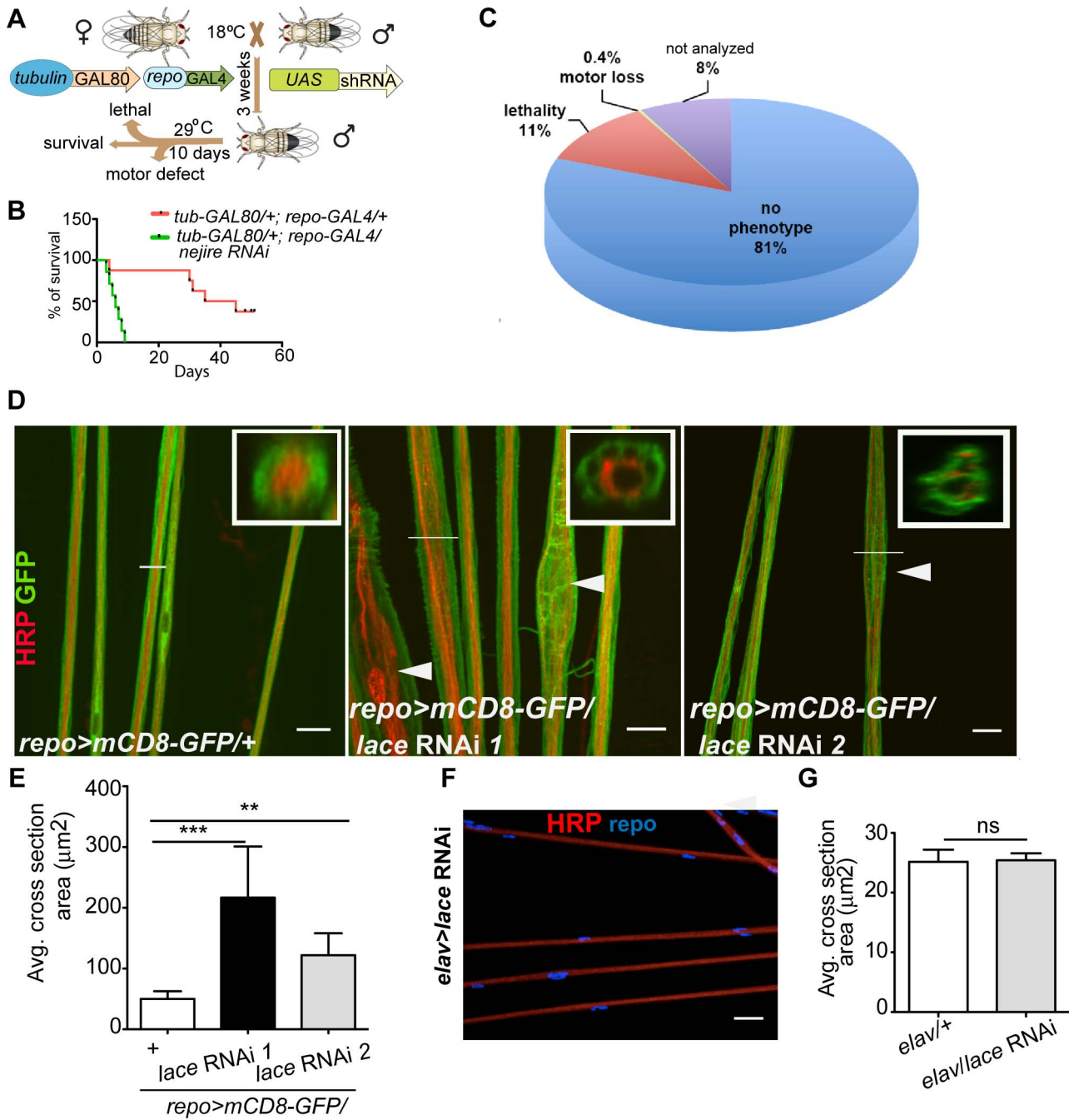


Figure 1. Primary screening and *lace* phenotype. (A) Scheme of the screening strategy. (B) Pre-screening result with *nejire* RNAi with *tub-GAL80^{ts}; repo-GAL4*. Survival curves were analyzed with Log-Rank Mantel Cox test. $p < 0.0001$ (C) Results from the primary screening reveal 861 RNAi lines with lethality and 30 RNAi lines with impaired locomotion. (D) Peripheral nerves of L3 larval PNS, glial membrane (green) swelling and axonal (red) wrapping defect were observed upon knockdown of *lace* with 2 different RNAi lines (Transformant ID 21803, 110181). *repo>mCD8-GFP/+* served as a control. Merged projection of confocal z-stacks is presented. In insets, orthogonal sections of the nerve region marked by a white line are shown (E) Quantification of the average cross-section of the peripheral nerves after glial specific knockdown of *lace*. (F) Merged projection of confocal z-stacks did not reveal any visible morphological changes in the neuronal morphology in the PNS after knockdown of *lace* specifically in the neurons (HRP). (G) Quantification of the average cross-section of the peripheral nerves after neuron-specific knockdown of *lace*. For the statistical analysis, unpaired *t*-test was performed with the respective control. Scale bar 20 μm . ns not significant. All graphs represent mean values \pm SD. ** $p < 0.01$ *** $p < 0.001$. doi:10.1371/journal.pgen.1003980.g001

expressing *UAS-lace* specifically in the glial cells (*repo-GAL4*), pointing to an essential function of *lace* in glia (Figure 2E,F).

Next, we analyzed, in which of the different glial subtype *lace* was required. Glia subtype specific *GAL4* drivers were used to

silence *lace* function. A phenotype was only observed when *lace* was depleted in wrapping glia (*Nrv2-GAL4*) (Figure 3A). Quantification of GFP signal intensity revealed that membrane area was significantly reduced as compared to control (*Nrv2>mCD8GFP/*

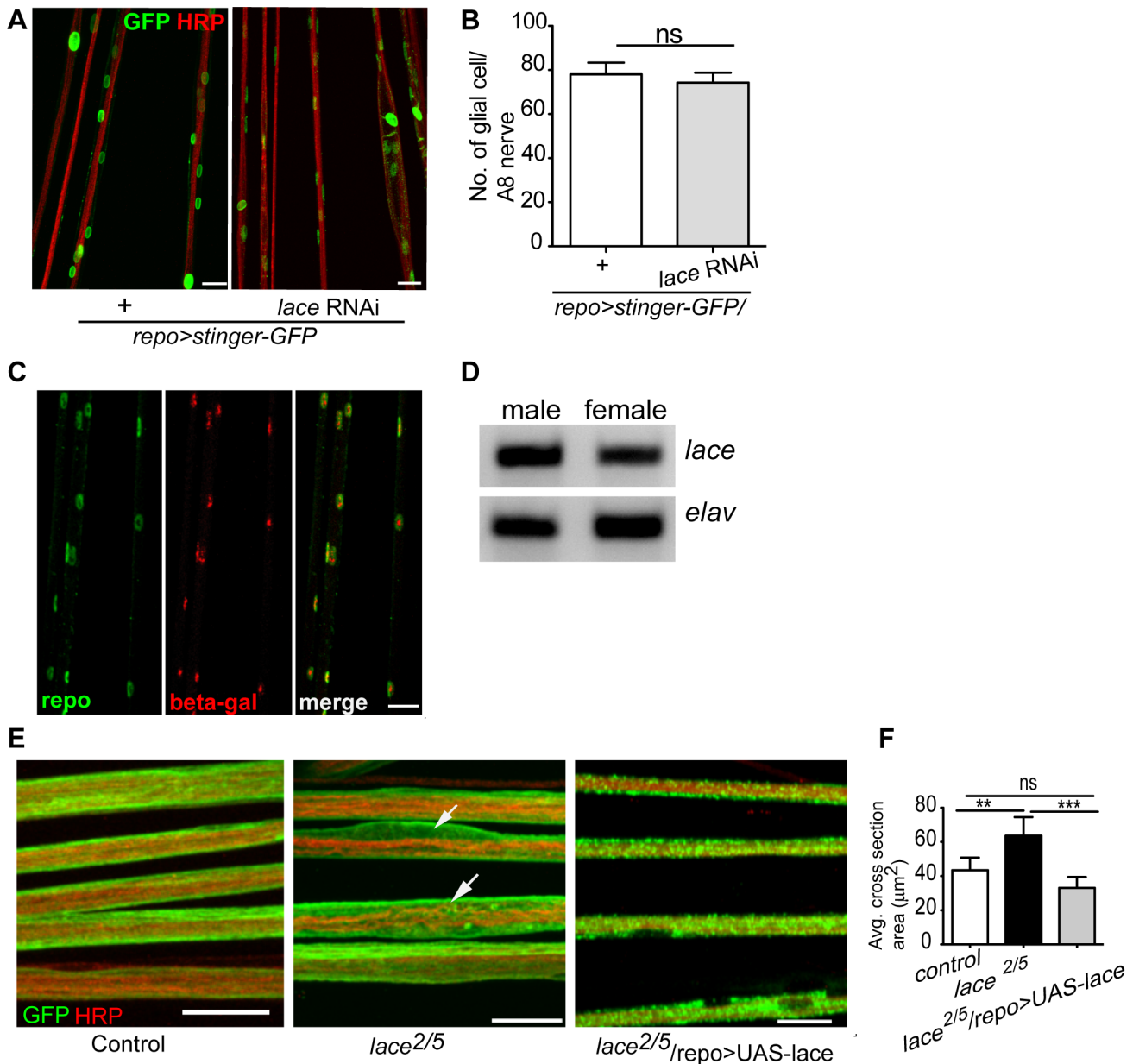


Figure 2. *lace* is expressed in glial cells. (A, B) Quantification of total glial cell number (mean ± SD) upon *lace* knockdown in glia. Counting the number of glial nuclei in A8 peripheral nerve (n=8) revealed no significant differences between control and *lace* RNAi larva. (C) Double immunolabeling of anti-β-galactosidase (red) and anti-repo (green) of *lace*⁵ (LacZ enhancer trap line) in L3 larval peripheral nerves. Colocalization shows that *lace* is expressed in glial cells, present in the peripheral abdominal nerves. (D) RT-PCR analysis showed that *lace* is expressed in the nervous system of both males and female flies. (E) Hypomorphic combination of *lace* mutant (*lace*²/*lace*⁵) showed axonal defasciculation and increase in the cross-section area of the nerve (arrows). HRP (red) and mCD8-GFP (green) were used to visualize the neuronal and glial morphology, respectively. (F) Quantification showed that the expression of *UAS-lace* by *repo-GAL4* could rescue the mutant phenotype. Scale bar 20 µm. All graphs represent mean values ± SD. Unpaired *t*-test (two groups) and One-way ANOVA followed by Tukey *post hoc* test (for three groups) were performed for the statistical analysis. Scale 20 µm. ** p<0.01 *** p<0.001. ns not significant. doi:10.1371/journal.pgen.1003980.g002

lace RNAi versus *Nrv2*>*mCD8GFP*) (Figure 3C). Similar results were observed when the *Nrv2*>*mCD8-mcherry* driver line was used to knockdown *lace* in the wrapping glia (Figure S5 A, E). In contrast, knockdown of *lace* in the two other glial subtypes, the subperineurial (*gliotactin-GAL4*) and the perineurial (*NP6293-GAL4*), did not lead to any visible changes (glial swellings or decrease in the GFP signal intensity) in glia or in axons (Figure S5A–G), suggesting a predominant role of *lace* in the encapsulation of peripheral nerves.

To examine the ultrastructure in more detail we performed electron microscopy. Electron micrographs clearly showed that knockdown of *lace* in glia (*repo/lace* RNAi) severely impaired axonal enwrapping compared to control (*repo/+*) (Figure 3B). Notably, also in the non-swollen regions (A2–A3 segment) of the nerve much less glial processes covered the axons. Quantification demonstrated a significant increase in the number of completely unwrapped axons in this region. We observed a similar phenotype, when *lace* was knocked down in wrapping glia (*Nrv2/lace* RNAi).

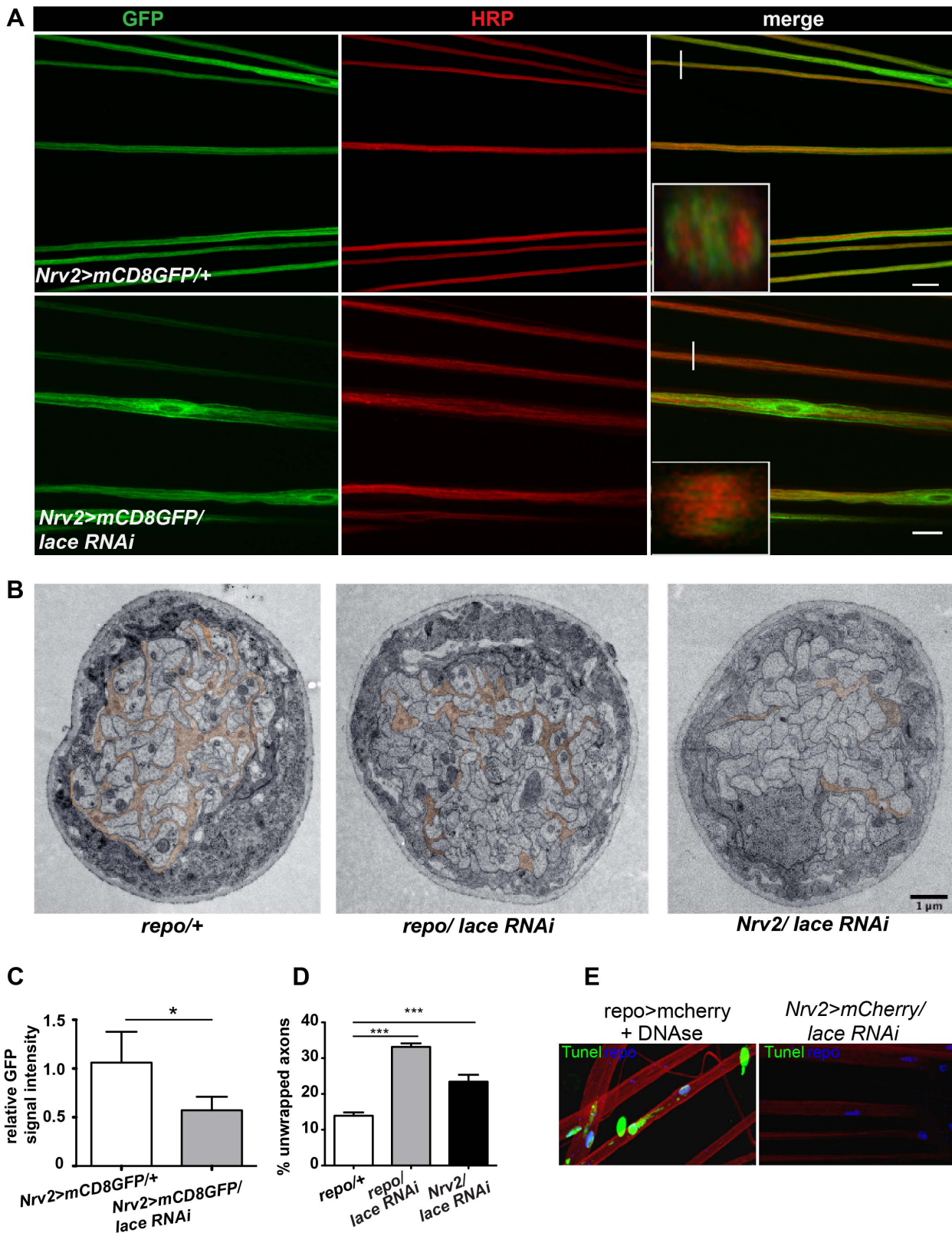


Figure 3. Wrapping glia require *lace* for axonal ensheatment. (A) *lace* RNAi was expressed specifically in wrapping glia (*Nrv2-GAL4*). mCD8-GFP (green) marks the membrane of wrapping glia and HRP (red) is used to visualize the neuronal membrane. Orthogonal sections from the non-swollen region are presented as insets. Scale 20 μ m. (B) TEM micrographs of L3 larval peripheral nerve cross-sections are shown. Wrapping glia is color-coded. Axonal ensheatment is incomplete upon loss of *lace* function in all glia (middle) or in wrapping glia (right). Proper ensheatment of axons is observed only in control (left). Scale 1 μ m. (C) Quantification of the GFP signal intensity of wrapping glial membrane was performed on merged confocal projections and t-test was used for the analysis. Scale 20 μ m. (D) Quantification of the number of unwrapped axons (8–10 nerves

from 4 animals for each genotype). One-way ANOVA followed by Dunnett *post hoc* test was performed. All graphs represent mean values \pm SD. * $p < 0.05$ *** $p < 0.001$. (E) TUNEL assay after *lace* knockdown in the wrapping glia and merged projection of the peripheral nerves are presented. TUNEL (green) positive nuclei are observed only in the positive control (after DNase addition). doi:10.1371/journal.pgen.1003980.g003

Again, a clear increase in the completely unwrapped axons was detected as compared to the controls (Figure 3D). Importantly, TUNEL assay could not detect any apoptotic glial nuclei (*Nrv2>laceRNAi*) suggesting that loss of axonal ensheathment is not because of dying wrapping glial cells (Figure 3E). Together, these results indicate that sphingolipids or intermediates of the sphingolipid pathway are necessary for membrane expansion of wrapping glia.

Ceramide-phosphoethanolamine is specifically required in wrapping glia

In order to search for the specific sphingolipid (SL) species required by the wrapping glia to mediate axonal ensheathment, a genetic dissection study was performed by expressing RNAi against all known SL metabolic enzymes selectively in glia [30]. Out of 12 genes, we found that knockdown of *Spt-I* [31], *schlank* [32], *Des1* [33] and *Pect* [34] in glia (*repo>mCD8-GFP/RNAi*) with two different RNAi lines (except *Des1* due to unavailability) phenocopied the glial swelling and axonal defasciculation as observed upon loss of *lace* function (Figure 4A, S6). Interestingly, all four genes that show 100% penetrance (Table S3) are known to be involved in the biosynthesis of ceramide-phosphoethanolamine (CerPE) (Figure 4B). The specificity of the effect was demonstrated by the absence of any visible phenotype after neuronal specific knockdown of *Spt-I*, *schlank*, *Des1* and *Pect*. (Figure 4C,D). Additionally, glial specific knockdown of different ceramide derivative synthesizing enzymes (*GlcTI*, *CGT*, *CerK*) [35,36] and PE synthesizing enzyme (*bbc*) [34] did not show any visible defects of axon or glial morphology (Figure S7). Moreover, when *Spt-I*, *schlank*, *Des1* or *Pect* were knocked down specifically in wrapping glia, wrapping defects similar to the *lace* phenotype were observed (Figure 5A). The quantification revealed that the GFP signal intensity was significantly reduced in all four experiments as observed after *lace* knockdown (Figure 5C,S8). Ultrastructural analysis by transmission electron microscopy also showed that wrapping glia failed to extend their membrane around the axons (Figure 5B); and consequently there was an increase of the completely unwrapped axons (Figure 5D). Hence, our data strongly suggests an essential function of glial CerPE in axonal ensheathment by wrapping glia.

In order to analyze whether knockdown of *lace*, *schlank*, *Des1* and *Pect* resulted in depletion of CerPE levels, we performed a detailed lipidomics analysis of the nervous system. This is particularly important in RNAi studies targeting enzymes, because residual enzyme activity due to inefficient RNAi-silencing is often sufficient for their function. Since the nervous system of *Drosophila* only contains 10% of glia, we expressed the RNAi both in neurons and glia using *repo-GALA* and *elav-GALA* drivers to deplete the enzymes in the entire nervous system. L3 larval brain and peripheral nerves were dissected and lipidomics analysis was performed with high-resolution shotgun mass spectrometry [37]. Importantly, our lipidomics analysis confirmed that knockdown of *lace*, *schlank*, *Des1* and *Pect* reduced CerPE levels significantly, whereas triacylglycerol (TAG) and diacylglycerol (DAG) and sterol levels were unaltered. Ceramide levels were reduced upon downregulation of *lace* and *Des1*, whereas knockdown of *Pect* lead to increased ceramide levels consistent with its function as a phosphoethanolamine cytidyltransferase. Phosphatidylcholines (PC) and Phosphatidylethanolamine (PE) levels

were slightly changed possibly due to compensatory mechanisms (Figure 6A–D).

To test the functional consequences of *lace* downregulation, we performed paired electrode recordings from abdominal nerves (Figure 7A) and determined the spike propagation velocities of afferent and efferent units (Figure 7B). We found that afferent spike propagation velocities are mildly decreased in *repo>mCD8-GFP/lace* RNAi mutants compared to *repo>mCD8-GFP/+* controls (median velocity smaller by 10.4%), whereas efferent spike propagation velocities remain unchanged (Figure 7C). The apparent reduction of afferent spike propagation velocities was confirmed by bootstrapping (Figure S9), which revealed that the medians of the velocity distributions obtained for *lace* RNAi flies and controls are significantly distinct ($p < 0.05$ (two-tailed), for efferent units $p > 0.4$).

Next, we tested whether it was possible to rescue the morphological phenotype induced by knockdown of *lace* in glia by supplementing sphingosine (re-converted to ceramide by condensation with a fatty-acylCoA catalyzed by the various ceramide synthases) into the diet of the flies. Indeed, the phenotype of glia-specific knockdown of *lace* was efficiently rescued by the exogenous addition of sphingosine (300 μ M) to the food (Figure 8). Double Immunolabelling of glia and neuronal membrane reveals that the glial bulging and axonal unpacking was rescued upon addition of sphingosine to the diet (Figure 8A). Orthogonal projections (Figure 8B) and the quantification demonstrated the rescue of the neuropathy like phenotype in flies (Figure 8C). We, furthermore, observed with the ultrastructural analysis that the glial enwrapment defect was recovered upon sphingosine addition to the diet (Figure 8D–E). Quantitative analysis of the peripheral nerves using the confocal and electron microscopy showed that the oral administration of sphingosine can restore the enwrapping defect and the neuropathy-like phenotype (Figure 8C,E).

Sphingolipids have both structural and signalling functions in cells. CerPE is a relatively low abundant lipid constituting only around 1% of the total fly lipidome. Interestingly, CerPE appears to be enriched in the fly brain membrane lipidome (4%) (Figure 4A) [37,38]. In mammals, CerPE is only found in trace amounts, since sphingolipids are in general built on ceramide phosphatidylcholine in higher organisms. There are different possibilities of how CerPE could exert its function in glia. CerPE might be required for signal transduction pathways that control membrane synthesis in wrapping glia. Recently, a mutation in egghead, an enzyme that extends the glycosphingolipids (GSLs) in flies, causes the proliferation and overgrowth of subperineurial glia mediated by aberrant activation of phosphatidylinositol 3-kinase-Akt pathway [39]. CerPE may also increase the packing density of the lipids in the membrane, thereby helping to build up an efficient barrier for the electrical insulation of the axons. In vertebrates, a related sphingolipid, galactosylceramide, is critical for the formation of an insulating myelin sheath in oligodendrocytes. Galactosylceramide and/or its sulphated form are required for the tight sealing of the glial paranodal membrane to the axon [40]. Interestingly, mice lacking ceramide synthase 2 [41], a vertebrate homolog of *schlank*, have myelination defects.

Alterations of enzyme function or enzyme deficiencies do not only result in a reduction in the amount of an essential product, but can also lead to the accumulation of a toxic intermediate, or the production of a toxic side-product. For example, mutations in human serine palmitoyltransferase result in a loss of normal

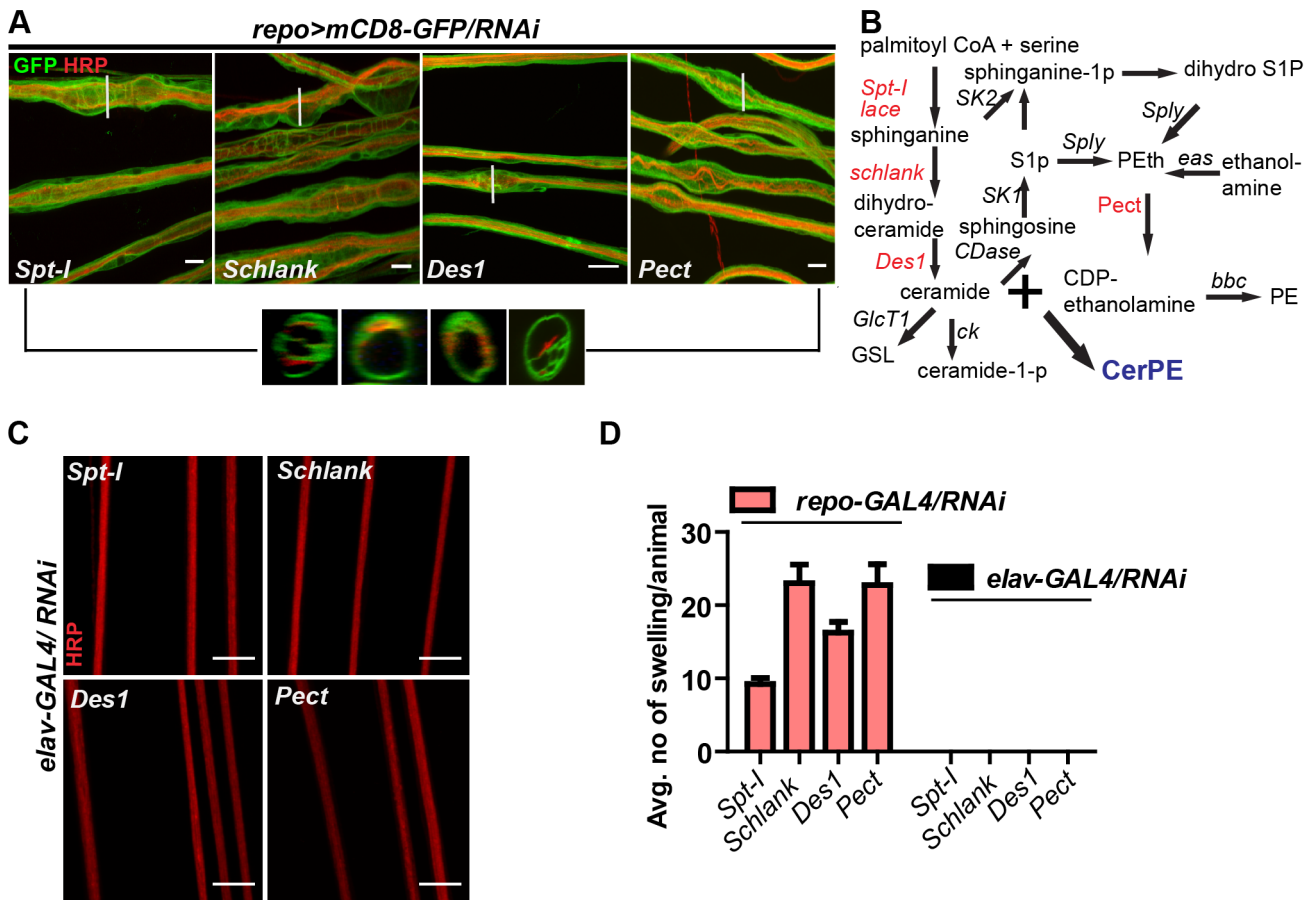


Figure 4. Glia require CerPE for axonal ensheathment. (A) A genetic dissection study of sphingolipid biosynthetic pathway shows that glial knockdown of *Spt-1*, *schlank*, *Des1* and *Pect* result in swelling and wrapping defects (*repo-GAL4*) similar to the *lace* phenotype. Merged projections of confocal stacks are presented. Scale 20 μ m. (B) Sphingolipid biosynthesis pathway. (C) RNAi against these 4 genes were expressed in neurons using *elav-GAL4* driver line. HRP (red) is used to visualize the membrane morphology of the neurons. Scale 20 μ m. (D) Quantification (mean \pm SD) showed that the swellings were only observed upon glial specific knockdown but not in neuron-specific knockdown. doi:10.1371/journal.pgen.1003980.g004

enzyme function causing a shift in the substrate specificity, which increase the accumulation of atypical, toxic lipid products [27]. Thus, gain-of-toxic-function is another possibility of how knockdown of *lace* may cause the axonal ensheathment defects.

Interestingly, supplementing sphingosine to the diet restored the ability of wrapping glia to extend their membrane around axons. How diets affect the distribution of lipids in cells and thereby modulate biological processes will be an important question for future investigations. *Drosophila* is an ideal system to pursue such studies because of the short life span and the powerful genetics, which enable rapid and detailed analysis. In summary, our current study illustrates that a large-scale screen in *Drosophila*, in combination with concomitant morphological and electrophysiological analysis has the potential to dissect the basic mechanisms of neuron-glia communication. Detailed knowledge of neuron-glia interactions is a pre-requirement for the rational design of treatment strategies for neuropathies or other diseases in the future.

Materials and Methods

Fly strains

Following lines were used in the study *w*[*]; *P*{*w*[+mC] = *nrv2-GAL4.S*}3 (in the text referred to as *Nrv2-GAL4*) [42], *w*[*]; *P*{*r182-GAL4*}/*CyO* (referred to as *Gliotactin-GAL4*) [43], *y*[*] *w*[*];

P{*w*[+mW.hs] = *GawB*}*Bsg*[*NP6293*]/*CyO*, *P*{*w*[-] = *UAS-lacZ*.*UW14*}/*UW14* (referred to as *NP6293-GAL4*) (DGRC,Japan) [44], *UAS-mCD8-GFP*, *UAS-stinger-GFP* (kindly provided by Christian Klämbt), *lace*⁵, *UAS-lace-HA* (kindly provided by Thomas Hummel) *w*[1118]; *P*{*w*[+mC] = *GAL4*} *repo*/TM3, *Sb* (referred to as *repo-GAL4*), *w*[*]; *P*{*w*[+mC] = *tub-P-GAL80*[*ts*]20; TM2/TM6B,Tb (referred to as *tub-GAL80^{ts}*), *P*{*w*[+mW.hs] = *GawB*}*elav*[*c155*] (referred to as *elav-GAL4*) (Bloomington Stock Center). For the screening, we generated a fly line (*w*; *tub-GAL80^{ts}*; *repo-GAL4*/TM3, *Sb*) referred to as *tub-GAL80^{ts}*; *repo-GAL4* by combining glial specific driver *repo-GAL4* with ubiquitously expressed temperature-sensitive allele of *GAL80^{ts}*. The RNAi library with predicted human orthologs was provided by VDRC based on common database (status October 2007). For the secondary screening and further morphological analysis, two different RNAi lines were obtained (GD and KK library). Two *lace* mutant lines *Adh*[*n7*] *lace*[2] *cn*[1] *vg*[1]/*CyO* (referred to as *lace*²), *y*[1] *w*[67c23]; *P*{*w*[+mC] = *lacW*}[45] *lace*[*k05305*]/*CyO* (referred to as *lace*³) (Bloomington Stock Center). Flies were provided with standard cornmeal-agar-yeast food if it is not mentioned otherwise.

Longevity assay

To deplete the mature glial cells *tub-GAL80^{ts}*; *repo-GAL4* flies were crossed with *UAS-nejire* RNAi, and *OregonR* (negative control).

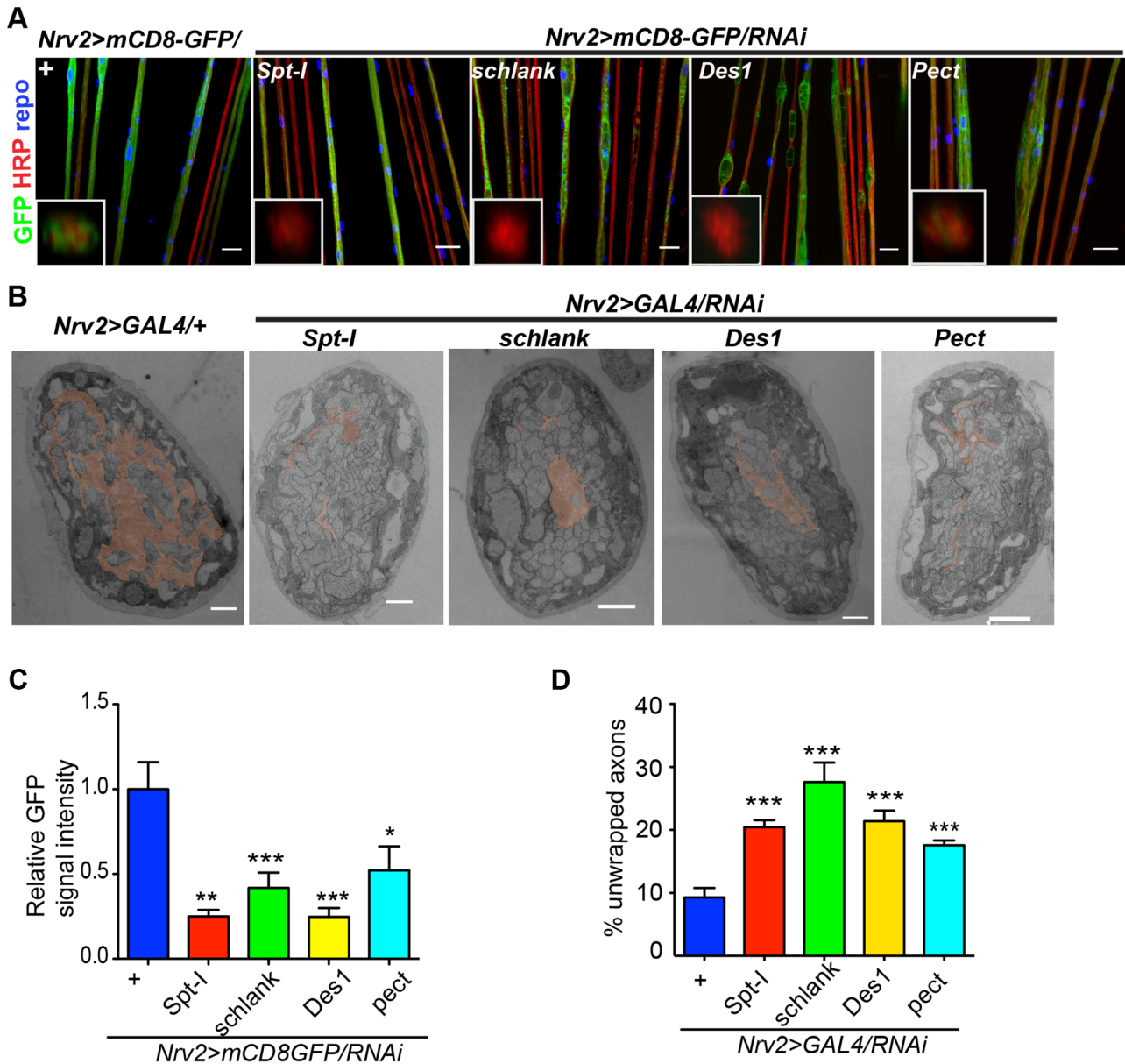


Figure 5. CerPE is very essential for axonal ensheathment by wrapping glia. (A) RNAi against *Spt-1*, *schlank*, *Des1* and *Pect* were expressed in wrapping glia (*Nrv2-GAL4*). Merged projections of the peripheral nerves along with an orthogonal projection are presented. GFP (green) was used to label the wrapping glial membrane, and HRP (red) and repo (blue) were used to label the neuronal membrane and glial nuclei, respectively. (B) TEM micrographs of L3 larval peripheral nerve cross-sections are shown. Wrapping glia is color-coded. Axonal ensheathment is incomplete upon loss of *lace* function in wrapping glia. Proper ensheathment of axons is observed only in control (+). Scale 1 μ m. (C) Quantification of GFP signal intensity of wrapping glial membrane showed a reduction of GFP signal intensity. (D) Quantification of the number of unwrapped axons. One-way ANOVA followed by Dunnett post hoc test was performed. All graphs represent mean values \pm 6 SD. * $p < 0.05$, ** $p < 0.01$, *** $p < 0.001$. doi:10.1371/journal.pgen.1003980.g005

3–4 days post-eclosion, adult males with the respective combination of GAL4-driver, UAS-transgene and GAL80^{ts} were shifted to 29°C (10–15 flies per vial). Numbers of dead flies were counted daily. After 2–3 days, fresh fly food was provided during the assay. At least 50 flies per genotype were used in the assay. Log Rank Test (Mantel-Cox) was used for statistical significance.

Immunohistochemistry

Drosophila L3 stage larva were dissected in 1× PBS (137 mM NaCl, 12 mM Phosphate, 2.7 mM KCl, pH 7.4) and the PNS fixed with Bouin’s fixative solution (HT10132, Sigma-Aldrich,

Germany for 3 min. Then the tissue was permeabilized with 1× PBT (0.1% Triton-X in PBS) solution for 15 min. For blocking (1 hour) and antibody dilutions 10% goat serum (G9023, Sigma-Aldrich, Germany) was used. Primary antibodies GFP (A11122, Invitrogen, Germany), anti-HRP-Cy3 (123-165-021, Dianova, Germany), antiHRP-alexa647 (123-605-021, Dianova, Germany), anti-repo (8D12, DSHB, University of Iowa, USA) were used with 1:1000, 1:200, 1:200, 1:20 dilutions, respectively. Primary antibodies were incubated overnight whereas secondary antibodies anti-rabbit alexa-488 (A-11008), mouse alexa-647 (A-21236, both from Invitrogen, Germany) mouse-Cy3 (115-165-14, Dianova,

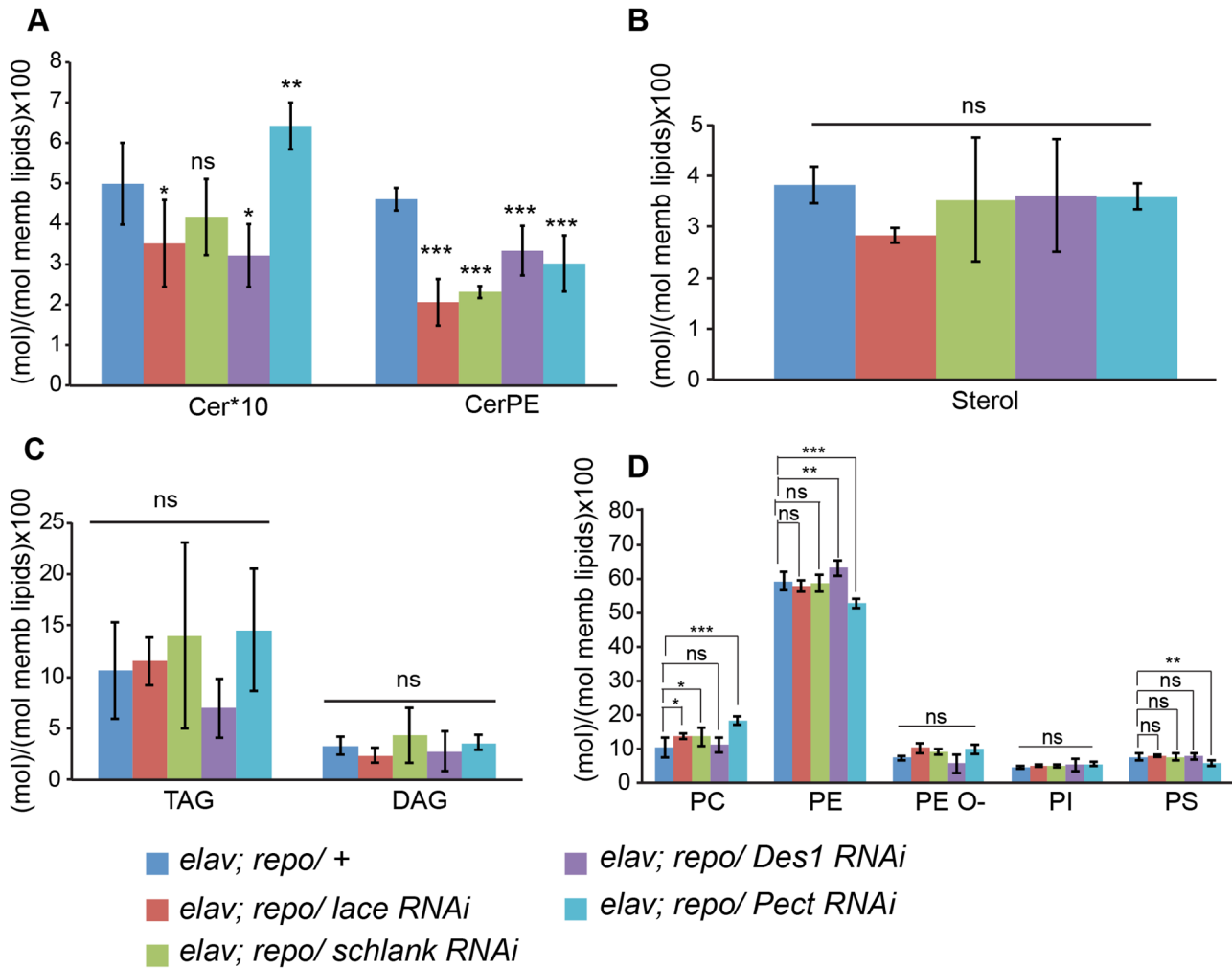


Figure 6. Lipidomics analysis. Lipidomics analysis using high-resolution shotgun mass spectrometry of dissected brains and peripheral nerves derived from L3 larvae. *lace*, *schlank*, *Des1* and *Pect* were downregulated in both neuron and glia, L3 larval brain and peripheral nerves were dissected and the amount of sphingolipid (A), sterol (B), neutral lipid (C) and phospholipids (D) were determined. One-way ANOVA with Dunnett *post hoc* test was used for the statistical analysis. All graphs represent mean values \pm SD. * $p < 0.05$ ** $p < 0.01$ *** $p < 0.001$. doi:10.1371/journal.pgen.1003980.g006

Germany) were used with 1:200 dilutions for 2 hours. After washing 3 times with PBT, larval mouth part was removed and fillets were mounted in Vectashield (H-1000, VectorLab, USA).

Quantification of *lace* phenotype

Approximately 200 μ m nerve segments were imaged from A3 or A4 body wall segment. Five nerve widths were measured approximately after every 40 μ m along the length of the nerve. Every five measurements of each nerve were considered as an ordered quintuplet (d_1, d_2, d_3, d_4, d_5) [46]. These five values were used to estimate average cross-sectional area of the nerve with the following equation:

$$A = (\pi/48)(d_1^2 + d_1d_2 + 2d_2^2 + d_2d_3 + 2d_3^2 + d_3d_4 + 2d_4^2 + d_4d_5 + d_5^2)$$

This estimated cross-sectional area of the nerve was calculated by considering the volume of the nerve same as that of a cylinder. At least 5–7 nerves per animals were used to measure this A-value.

A-values from each animal were averaged and the mean of these average values were compared between control and *lace* knock-down.

Quantification of wrapping glia phenotype

For the analysis of wrapping glia defects, *Nrv2-GAL4* line was crossed with different *UAS-shRNA* lines. Images of L3 larval stage PNS were taken for both control and treated groups with exactly the same settings of the confocal microscope (Zeiss, LSM 510). Quantification of the intensity was performed using ImageJ software (NIH, USA). The intensity of the signal was measured as the mean grey value per square micrometer.

Confocal microscopy

L3 larval PNS was imaged with Zeiss confocal microscope (LSM510) having 40 \times water-immersion objective. z-stacks images with optical section of 0.5 μ m were taken and digital projections of the stack and optical orthogonal section was analyzed using Zeiss LSM image browser software. ImageJ was used for the image processing.

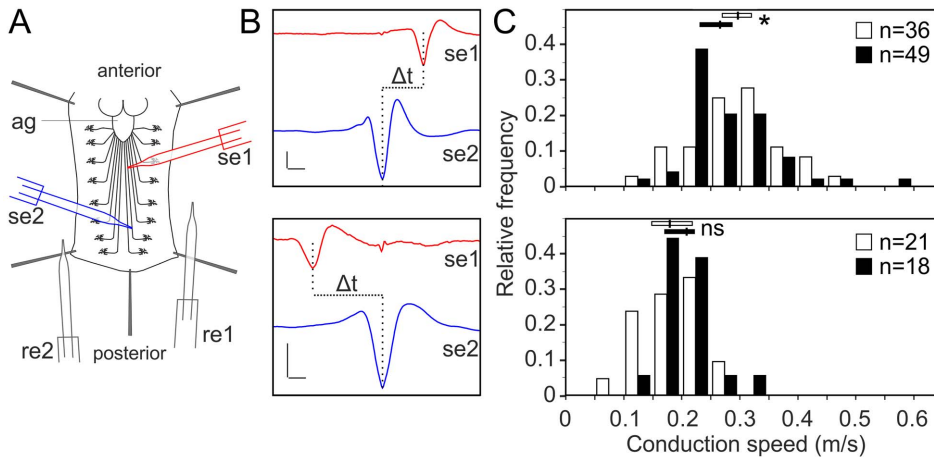


Figure 7. Glial inhibition of *lace* delays afferent spike propagation. (A) Scheme of thoracic and abdominal parts of a dissected larva, electrodes not to scale; ag abdominal ganglion mass, se1, re1 anterior suction electrode and reference electrode, se2, re2 posterior suction electrode and reference electrode. (B) Afferent unit (top) and efferent unit (bottom) recorded simultaneously in 7th right nerve of a *repo>mCD8-GFP/+* control as sketched in (A). Spike templates were generated for se2 and served as trigger events for averaging both se1 and se2. Δt conduction time; bars 50 μ V and 1 ms, respectively. (C) Distribution of conduction speed recorded in *repo>mCD8-GFP/+* (white bars) and *repo>mCD8-GFP/lace RNAi* (black bars) animals from afferent (top) and efferent (bottom) units. Horizontal lines indicate medians and their 95% confidence interval of the respective distributions. Difference of medians: * $p < 0.05$ (two-tailed), ns not significant. n number of neurons, recorded from 20 mutant and 9 control larvae. doi:10.1371/journal.pgen.1003980.g007

RT-PCR

Drosophila larval brain and PNS was dissected and total RNA was isolated using Macherey Nagel (Germany) RNA isolation kit according to the manufacturer protocol.

1 μ g of RNA was used for cDNA synthesis using SuperScript III First-Strand synthesis kit (18080-051, Invitrogen, Germany). 1 μ g RNA, 1 μ l of 50 μ M oligo(dT)20, 1 μ l of 10 mM dNTP mix and sterile water were mixed to make up volume to 10 μ l. The mixture was incubated at 65°C for 5 min and then cooled down to 4°C. A Reverse Transcriptase mix (RT mix) was prepared by mixing 2 μ l 10 \times RT buffer, 4 μ l 25 mM MgCl₂, 2 μ l 0.1 M DTT, 1 μ l RNaseOUT and 1 μ l Superscript III RT. All of the reagents were provided in kit. RT mix was added to pre-cooled RNA-mix and incubated for 50 min at 50°C. The reaction was stopped by increasing the temperature to 85°C for 5 min. 1 μ l RNase H was added and incubated for 20 min at 37°C to cleave remaining RNA. The mixture was cooled to 4°C and cDNA samples were stored at -20°C. cDNA samples were used as template to do a normal semi-quantitative PCR. 2 μ l cDNA (1:10 dilution), 0.3 μ l of each primer, 2.5 μ l of 25 mM MgCl₂, 1 μ l 10 mM dNTP, 10 μ l 5 \times GoTaq flexi reaction buffer, 0.2 μ l of Go-Taq flexi DNA polymerase (M8301, Promega, Germany) were mixed and sterile water was added to make final volume 50 μ l. Primers for *elav* are 5'-CGCACAAACCTTATTGTCAACTAC-3' and 5'-AATTTTACCACATATGGGGTCTGTG-3'. Primers for *lace* are 5'-TTCGACGGCGATTCTGGAAC-3' and 5'-CAGAGCAATAACCTCGGGCAAA-3'.

Electron microscopy

For all our experiments, we chose the very late third instar larva namely, wandering L3 larva that stopped eating and climbed away from the food. All larva for the analysis were collected 6 days after egg laying at 25°C. Larval fillets were fixed with a mixture of 4% paraformaldehyde and 2.5% glutaraldehyde in 0.1 M PBS for 4 hours at room temperature. The fillets were washed with PBS and then subjected to post-fixation with 1% osmium tetroxide for 1 hour at 4°C. Next, the post-fixed fillets were dehydrated and stained with a mixture of freshly prepared 1.5% uranyl acetate and

1.5% tungstophosphoric acid. After completion of dehydration process, the fillets were embedded in Epon. Then the silver sections (from A2–A3 regions) were cut and contrasted with 4% uranyl acetate followed by 0.3% lead citrate. Multiple sections were cut, contrasted and imaged for every genotype. The sections were imaged with a LEO EM912 Omega electron microscope (Carl Zeiss, Germany) and the digital micrographs were obtained with an on-axis 2048X2048 CCD camera (Proscan GmbH, Germany).

Spike propagation velocities

Paired suction electrode recordings of spontaneous spiking activity (20°–23°C, HL3 saline [45]) obtained at the same abdominal nerve in fillet dissection were band-pass filtered (100–3000 Hz) and simultaneously sampled at a rate of 20 kHz. Waveform templates generated with Spike II (Cambridge Electronics, UK) were used as triggers for averaging both electrode signals. Electrode tips were placed on approximately the same z-level and photographed to assess their tip-to-tip distance. Action potential speed distributions were compared by bootstrapping using 10000 repetitions to reveal the 95% confidence intervals of the medians in the two experimental groups.

Lipidomics analysis

L3 larval brain and peripheral nerves were dissected and then processed for lipid isolation and mass-spectrometry analysis as described before [37]. Briefly, for each replicate, 5 brains were homogenized in 150 mM ammonium bicarbonate using a pestle attached to a cordless motor. For each knockdown experiment, samples were collected from the crossing of three different parents.

Sample volume was adjusted to 200 μ l. For absolute quantification, internal standards were added to control for lipid-class dependent differences in extraction and ionization. The internal standard mix contained PG 17:0 and TAG 36:0, 10 pmol; Cer 17:0, GalCer 12:0 and DAG 17:0, 20 pmol; PA 17:0, 25 pmol; PS 17:0 and PC 18:3, 40 pmol; PI 17:0, CerPE 12:0, Chol-D7 and PE 17:0, 50 pmol. Lipids were extracted using a modified Folch extraction protocol [47]: 265 μ l of methanol was added to the

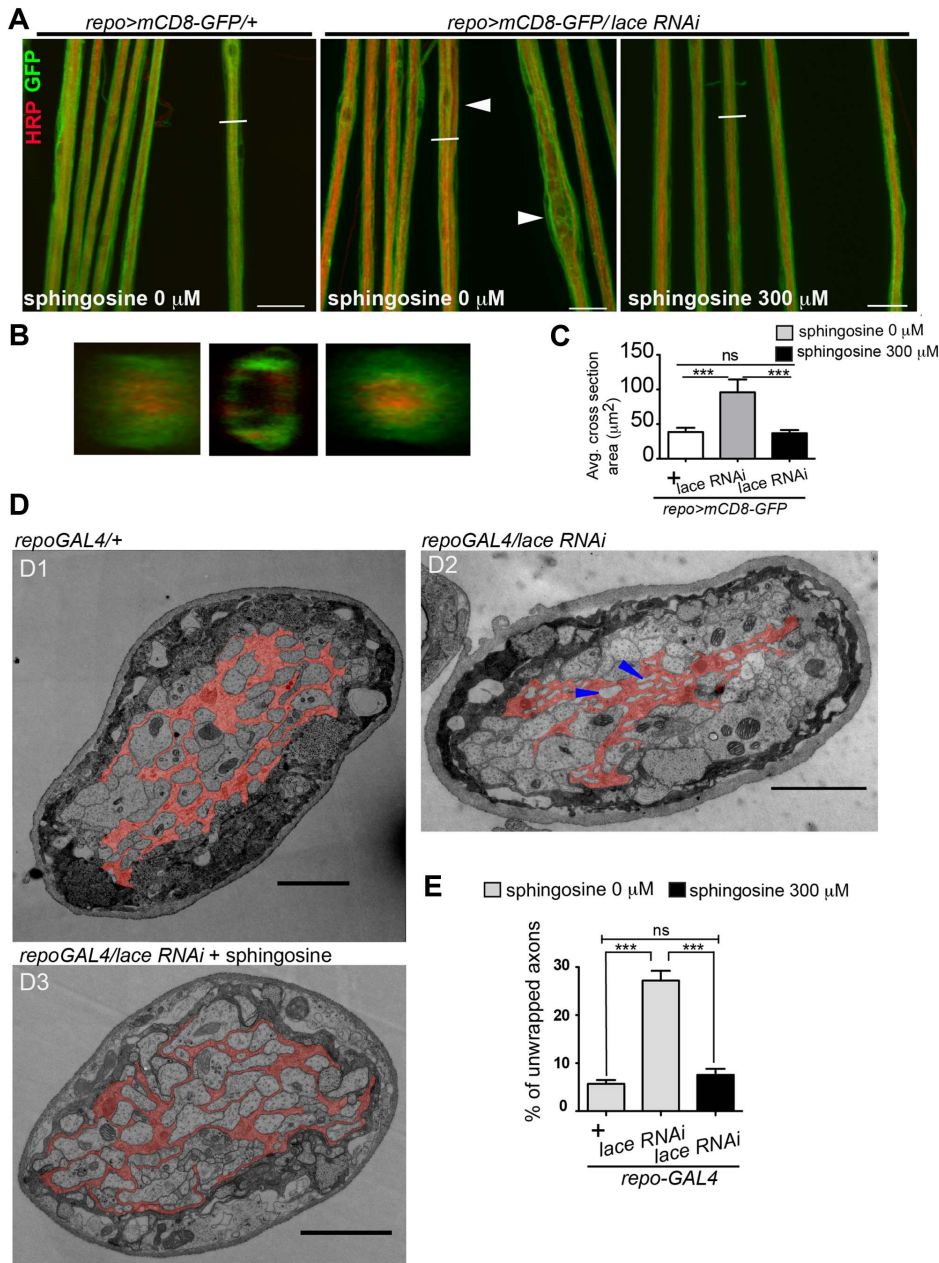


Figure 8. Spingosine rescues the glial bulging phenotype. (A) Addition of sphingosine to diet rescues the *lace* phenotype. Arrowheads indicate glial swelling region. (B) Orthogonal projections showed that dietary addition of sphingosine rescues the ensheathment defect. (C) Quantification of average cross-section area after knockdown of *lace* in glia and upon sphingosine treatment is shown. All graphs represent mean values \pm SD. One-way ANOVA followed by Tukey *post hoc* test was performed for statistical analysis. Scale 20 μ m (D1–D3) TEM micrographs of L3 larval peripheral nerve cross-sections are shown. Wrapping glia is color-coded. Vacuoles (blue arrowhead) are present in the wrapping glia and there is loss of membrane extension resulting in lack of proper ensheathment in *repo-GAL4/lace RNAi* flies as compared to control *repo-GAL4/+* flies. (D3) Addition of 300 μ M sphingosine to the diet (Matreya, USA) rescues the ensheathment defect. (E) Quantification of the number of unwrapped axons before and after sphingosine treatment in the *lace* knocked down flies. (*repo-GAL4/laceRNAi*). One-way ANOVA followed by Tukey *post hoc* test was performed. All graphs represent mean values \pm SD. *** $p < 0.001$. doi:10.1371/journal.pgen.1003980.g008

aqueous phase and vortexed; 730 μ l of chloroform was added and the samples were vortexed for 1 h; after centrifugation, the organic phase was collected and dried under vacuum to avoid lipid oxidation. The whole extraction procedure including sample preparation was performed at 4°C in order to prevent lipid degradation. All lipid standards were purchased from Avanti Polar Lipids (Alabaster, USA). Solvents were purchased from Sigma-Aldrich (Taufkirchen, Germany).

Mass spectrometric analyses were performed on a QExactive instrument (Thermo Fisher Scientific, Germany) equipped with a robotic nanoflow ion source TriVersa NanoMate (Advion BioSciences, Ithaca, USA) using chips with the diameter of spraying nozzles of 4.1 μ m. The ion source was controlled by Chipsoft 8.3.1 software. Ionization voltages were +1.25 kV and -0.9 kV in positive and negative modes, respectively; back-pressure was set at 0.95 psi in both modes. The temperature of ion

transfer capillary was 200°C; tube voltages were 90 V (MS+) and -150 V (MS-). Acquisitions were performed at the mass resolution $R_{m/z\ 200} = 140\ 000$. AGC control was set at 10^6 ions and maximum injection time was set to 50 ms.

Dried total lipid extracts were re-dissolved in 100 μ l of chloroform:methanol 1:2. For the analysis, 10 μ l of samples were loaded onto 96-well plate (Eppendorf, Germany) of the TriVersa NanoMate ion source and sealed with aluminium foil. Each sample was analyzed for 4 min in positive ion mode where PE, PC, PC-O, TAG, CerPE and DAG were detected and quantified. This was followed by an acquisition in negative ion mode for 5 min where PA, PI, PS, PG, PE, PEO-, Cer, HexCer were detected and quantified.

Sterol quantification method was performed as described elsewhere [37]. Briefly, dried samples were sulfated with sulfur trioxide pyridine complex in pyridine (Sigma-Aldrich, Germany), sonicated and incubated at room temperature. Then barium acetate (Sigma-Aldrich, Germany) was added, samples sonicated and incubated 10 min at room temperature and then 1 hour at 4°C. Sulfated sterols were quantified in MS mode on QExactive mass spectrometer using cholesterol-D7 (Avanti Polar Lipids, USA) as internal standard.

Lipids were identified by LipidXplorer software [48] by matching the m/z of their monoisotopic peaks to the corresponding elemental composition constraints. Mass tolerance was 5 p.p.m and intensity threshold was set according to the noise level reported by Xcalibur software (Thermo Scientific, Germany).

Dye penetration assay

In order to check the integrity of blood nerve barrier, third instar larva were injected with dextran conjugated Rhodamine dye using standard procedure [49,50]. 10 kD dextran conjugated Rhodamine was injected in the third instar larval abdominal cavity using a FemtoJet express microinjecting device (Eppendorf). For the injections, glass micropipettes prepared with a P-97 pipette puller (Sutter Instrument) from glass tubes (thin wall, 3 inches, 1-mm diameter; World Precision Instruments) were used. Injection was monitored using a dissection microscope (Leica MZ6). The successful injections were monitored using a stereomicroscope (Zeiss).

After the injections, animals were kept in small Petridis with standard fly food so that they can eat and move. 20–30 min post injection live animals were placed under the microscope after a brief cold shock. Confocal images of larval ventral cord and peripheral nerves were acquired using a Zeiss 510 Confocal microscope.

TUNEL assay

Terminal deoxynucleotidyl transferase- mediated biotinylated UTP nick end labeling (TUNEL) was performed to detect the wrapping glial apoptosis. In situ cell death detection kit (Roche) was used for the assay and was performed according to the manufacturer protocol.

Supporting Information

Figure S1 Results of GMR screening. (A) Candidates from primary screening were compared when crossed with GMR-GAL4 to express the RNAi specifically in the eye. The screen resulted in lethality in 3.5% of the flies, whereas 12.4% of the RNAi lines showed a morphological alteration of the red eye (rough eye phenotype). 84.1% RNAi lines did not show any visible defects in the red eye morphology. Images of control flies (GMR-GAL4) (B) and different rough eye phenotypes (C) are presented. (TIF)

Figure S2 STRING protein association network of lipid and carbohydrate metabolism candidates. Based on the prediction of the STRING protein association database, primary hits of lipid and carbohydrate metabolism are analyzed for their predicted functional associations. Based on this networking, hits that are likely to be associated with three or more candidates (red) are chosen for the secondary screening analysis. The nomenclature is given for *Drosophila* hits and their predicted human ortholog. (TIF)

Figure S3 Phenotypes of the secondary screening with the selected metabolic candidates. *UAS-RNAi* was expressed using pan-glial driver *repo-GAL4* and the effects were visualized in L3 larval PNS. Different phenotypes that are observed are shown in the figure. A detailed description of the phenotypes is presented in Table S2. Glial membrane was imaged by expressing *UAS-mCD8-GFP* (green). HRP (red) stained neuronal membrane. Merged projection of all z-stacks is presented in the panel. As a control, the driver line was crossed with wild type. Scale bar 20 μ m. (TIF)

Figure S4 Blood-Nerve-Barrier (BNB) was not compromised. (A) 10 kD Dextran-conjugated Rhodamine dye (red) was injected in the L3 larva. Confocal z-stack of the peripheral nerves (green) and ventral nerve cord show no penetration of the dye in the nervous system. (B) TEM analysis showed no alteration of septate junction morphology. (TIF)

Figure S5 Glial bulging phenotype was specific to the wrapping glia. *lace* RNAi was expressed specifically in wrapping glia using two different driver line *Nrv2-GAL4* (A-A'), in subperineurial glia (*ghiotactin-GAL4*) (B) and in perineurial glia (*NP6293-GAL4*) (C). For the visualization of wrapping glial membrane, mCD8-mcherry and 6STGFP was expressed with *Nrv2-GAL4* driver while mCD8-GFP was expressed to visualize the subperineurial and perineurial glial membrane. Merged projections of confocal z-stacks are represented. HRP (red) immunolabelling was performed to observe the axonal morphology. (D) Average number of swelling regions were quantified in each knockdown experiment and respective driver lines were used as control (n=8 for each genotype). Swellings were observed upon knockdown of *lace* only in the wrapping glia. The graph represents the mean values + SD. (E–G) Quantification of signal intensity of mcherry and GFP are shown. mcherry level was significantly reduced upon knockdown of *lace* by *Nrv2-GAL4* whereas GFP signal intensity was unchanged upon *lace* knockdown in subperineurial (*Gli/lace* RNAi) and perineurial glia (*NP6293/lace* RNAi). 10–12 nerves per animal (n=8) were imaged for the quantification. Scale 20 μ m. (TIF)

Figure S6 Knockdown of *Spt-I*, *schlank*, *Pect* with a second RNAi using *repo-GAL4*. (A) Projection of all confocal stacks after immunolabeling with GFP and HRP shows glial swelling. (B) Orthogonal section of the nerve region marked in white shows axonal defect (red) and glial membrane (green). Repo labels glial nuclei (blue). Scale bar 20 μ m. (TIF)

Figure S7 Glia-specific knockdown of two essential genes in GSL biosynthesis pathway. *GlcT1* and *CGT*, each with two different RNAi driven by *repo-GAL4*, show no visible changes in glial (green) and axonal (red) morphology. *Ceramide Kinase* (CK) knockdown using *repo-GAL4* is also without any obvious phenotype. Glial specific (*repo-GAL4*) knockdown of *bbc*, an essential gene in PE biosynthesis, with two different RNAi (VDRC) does not

result in visible effects on axonal (red) and glial (green) morphology. Scale bar 20 μm . (TIF)

Figure S8 Knockdown of *Spt-I*, *schlank*, *Des1* and *Pect* affects axonal wrapping. The analysis of the GFP signal intensity along the peripheral nerve after knockdown of *Spt-I*, *schlank*, *Des1* and *Pect* in wrapping glia (*Nrv2>mCD8GFP/RNAi*) as compared to the control (*Nrv2>mCD8GFP/+*). (TIF)

Figure S9 Bootstrap analysis of spike propagation velocity differences after *lace* knockdown. Bootstrap statistics for comparing median afferent (left) and efferent (right) spike propagation velocities between *repo>mCD8-GFP/lace RNAi* mutants and *repo>mCD8-GFP/+* controls. Data were resampled 10000 times to compute differences of medians ($\text{median}_{\text{control}} - \text{median}_{\text{laceRNAi}}$). Black trace: sorted differences; ordinates are scaled to cover the whole range of resampled differences obtained. Red line: difference of medians obtained from the original data sets. Green line: mean of the 10000 resampled differences of medians. Blue lines: 95% confidence range of the resampled differences (i.e. 250 samples generated smaller differences and 250 samples generated larger differences, respectively). As this confidence range includes zero for efferent axons (right), there is no significant difference of median conduction speed between mutants and controls. By contrast, the confidence range excludes zero for afferent axons (left), signalling a significantly altered conduction speed in sensory cells of mutant larvae. Multiple repetition of this resampling procedure yielded p values between 0.0336 and 0.366 (mean $p = 0.0356$, for two-tailed test). If the test hypothesis is reformu-

lated ("is conduction speed reduced in *lace RNAi* specimens compared to controls?"), the one-tailed test rejects the null hypothesis with $p < 0.02$, in spite of the numerically small difference of the median conduction speeds (0.0318 m/s) observed in the recordings from afferent units. (TIF)

Table S1 List of candidates with glial essential function. (XLSX)

Table S2 Results of the secondary screening using genes from lipid and carbohydrate metabolic pathways. (XLSX)

Table S3 Genetic dissection of *lace* phenotype using sphingolipid biosynthetic enzymes. (XLS)

Acknowledgments

We are grateful to C. Klämbt and T. Hummel for advice and fly lines. We are thankful to A. Denker and S. Rizzoli for the help with dextran injection assay. We thank Developmental Studies Hybridoma Bank, Vienna Drosophila RNAi Center and Bloomington Stock Center for providing us antibodies; RNAi fly lines and general fly stocks, respectively.

Author Contributions

Conceived and designed the experiments: AG MS. Performed the experiments: AG TK NS JLS HG BG. Analyzed the data: AG TK NS JLS HG BG MS MCG. Contributed reagents/materials/analysis tools: AV JBS AS MCG. Wrote the paper: AG MS.

References

- Freeman MR, Doherty J (2006) Glial cell biology in Drosophila and vertebrates. *Trends Neurosci* 29: 82–90.
- Barres BA (2008) The mystery and magic of glia: a perspective on their roles in health and disease. *Neuron* 60: 430–440.
- Sherman DL, Brophy PJ (2005) Mechanisms of axon ensheathment and myelin growth. *Nat Rev Neurosci* 6: 683–690.
- Mirsky R, Jessen KR (1996) Schwann cell development, differentiation and myelination. *Curr Opin Neurobiol* 6: 89–96.
- Kretschmar D, Hasan G, Sharma S, Heisenberg M, Benzer S (1997) The Swiss cheese mutant causes glial hyperwrapping and brain degeneration in Drosophila. *J Neurosci* 17: 7425–7432.
- Pohl HBF, Porcheri C, Mueggler T, Bachmann LC, Martino G, et al. (2011) Genetically induced adult oligodendrocyte cell death is associated with poor myelin clearance, reduced remyelination, and axonal damage. *J Neurosci* 31: 1069–1080.
- Buch T, Heppner FL, Tertilt C, Heinen TAJ, Kremer M, et al. (2005) A Cre-inducible diphtheria toxin receptor mediates cell lineage ablation after toxin administration. *Nat Methods* 2: 419–426.
- Edwards TN, Meinertzhagen IA (2010) The functional organisation of glia in the adult brain of Drosophila and other insects. *Progress in neurobiology* 90: 471–497.
- Booth GE, Kinrade EF, Hidalgo A (2000) Glia maintain follower neuron survival during Drosophila CNS development. *Development* 127: 237–244.
- Vossfeldt H, Butzlaff M, Prussing K, Ni Charthaigh RA, Karsten P, et al. (2012) Large-scale screen for modifiers of ataxin-3-derived polyglutamine-induced toxicity in Drosophila. *PLoS One* 7: e47452.
- Dietzl G, Chen D, Schnorrer F, Su K-C, Barinova Y, et al. (2007) A genome-wide transgenic RNAi library for conditional gene inactivation in Drosophila. *Nature* 448: 151–156.
- Lee BP, Jones BW (2005) Transcriptional regulation of the Drosophila glial gene repo. *Mech Dev* 122: 849–862.
- Sepp KJ, Schulte J, Auld VJ (2001) Peripheral glia direct axon guidance across the CNS/PNS transition zone. *Dev Biol* 238: 47–63.
- McGuire SE, Le PT, Osborn AJ, Matsumoto K, Davis RL (2003) Spatiotemporal rescue of memory dysfunction in Drosophila. *Science* 302: 1765–1768.
- Maere S, Heymans K, Kuiper M (2005) BiNGO: a Cytoscape plugin to assess overrepresentation of gene ontology categories in biological networks. *Bioinformatics* 21: 3448–3449.
- Funfschilling U, Supplie LM, Mahad D, Boretius S, Saab AS, et al. (2012) Glycolytic oligodendrocytes maintain myelin and long-term axonal integrity. *Nature* 485: 517–521.
- Lee Y, Morrison BM, Li Y, Lengacher S, Farah MH, et al. (2012) Oligodendroglia metabolically support axons and contribute to neurodegeneration. *Nature* 487: 443–448.
- Xie X, Auld VJ (2011) Integrins are necessary for the development and maintenance of the glial layers in the Drosophila peripheral nerve. *Development* 138: 3813–3822.
- Stork T, Engelen D, Krudewig A, Silies M, Bainton RJ, et al. (2008) Organization and function of the blood-brain barrier in Drosophila. *J Neurosci* 28: 587–597.
- Parker RJ, Auld VJ (2004) Signaling in glial development: differentiation migration and axon guidance. *Biochem Cell Biol* 82: 694–707.
- Banerjee S, Bhat MA (2008) Glial ensheathment of peripheral axons in Drosophila. *J Neurosci Res* 86: 1189–1198.
- Sepp KJ, Schulte J, Auld VJ (2000) Developmental dynamics of peripheral glia in Drosophila melanogaster. *Glia* 30: 122–133.
- Lee T, Luo L (1999) Mosaic analysis with a repressible cell marker for studies of gene function in neuronal morphogenesis. *Neuron* 22: 451–461.
- Snel B, Lehmann G, Bork P, Huynen MA (2000) STRING: a web-server to retrieve and display the repeatedly occurring neighbourhood of a gene. *Nucleic Acids Res* 28: 3442–3444.
- Hanada K (2003) Serine palmitoyltransferase, a key enzyme of sphingolipid metabolism. *Biochim Biophys Acta* 1632: 16–30.
- Dawkins JL, Hulme DJ, Brahmabhatt SB, Auer-Grumbach M, Nicholson GA (2001) Mutations in SPTLC1, encoding serine palmitoyltransferase, long chain base subunit-1, cause hereditary sensory neuropathy type I. *Nat Genet* 27: 309–312.
- Rothier A, Penno A, Rautenstrauss B, Auer-Grumbach M, Stettner GM, et al. (2011) Characterization of two mutations in the SPTLC1 subunit of serine palmitoyltransferase associated with hereditary sensory and autonomic neuropathy type I. *Hum Mutat* 32: E2211–2225.
- Leiserson WM, Harkins EW, Keshishian H (2000) Fray, a Drosophila serine/threonine kinase homologous to mammalian PASK, is required for axonal ensheathment. *Neuron* 28: 793–806.
- Adachi-Yamada T, Gotoh T, Sugimura I, Tateno M, Nishida Y, et al. (1999) De novo synthesis of sphingolipids is required for cell survival by down-regulating c-Jun N-terminal kinase in Drosophila imaginal discs. *Mol Cell Biol* 19: 7276–7286.
- Dobrosotskaya IY, Seegmiller AC, Brown MS, Goldstein JL, Rawson RB (2002) Regulation of SREBP processing and membrane lipid production by phospholipids in Drosophila. *Science* 296: 879–883.
- Chintapalli VR, Wang J, Dow JAT (2007) Using FlyAtlas to identify better Drosophila melanogaster models of human disease. *Nat Genet* 39: 715–720.

32. Bauer R, Voelzmann A, Breiden B, Schepers U, Farwanah H, et al. (2009) Schlank, a member of the ceramide synthase family controls growth and body fat in *Drosophila*. *EMBO J* 28: 3706–3716.
33. Basu J, Li Z (1998) The Des-1 protein, required for central spindle assembly and cytokinesis, is associated with mitochondria along the meiotic spindle apparatus and with the contractile ring during male meiosis in *Drosophila melanogaster*. *Mol Gen Genet* 259: 664–673.
34. Lim H-Y, Wang W, Wessells RJ, Ocorr K, Bodmer R (2011) Phospholipid homeostasis regulates lipid metabolism and cardiac function through SREBP signaling in *Drosophila*. *Genes & Development* 25: 189–200.
35. Kohyama-Koganeya A, Sasamura T, Oshima E, Suzuki E, Nishihara S, et al. (2004) *Drosophila* glucosylceramide synthase: a negative regulator of cell death mediated by proapoptotic factors. *J Biol Chem* 279: 35995–36002.
36. Dasgupta U, Bamba T, Chiantia S, Karim P, Tayoun ANA, et al. (2009) Ceramide kinase regulates phospholipase C and phosphatidylinositol 4, 5, bisphosphate in phototransduction. *PNAS* 106: 20063–20068.
37. Carvalho M, Sampaio JL, Palm W, Brankatschk M, Eaton S, et al. (2012) Effects of diet and development on the *Drosophila* lipidome. *Mol Syst Biol* 8: 600.
38. Guan XL, Cestra G, Shui G, Kuhrs A, Schittenhelm RB, et al. (2013) Biochemical membrane lipidomics during *Drosophila* development. *Dev Cell* 24: 98–111.
39. Dahlgaard K, Jung A, Qvortrup K, Clausen H, Kjaerulff O, et al. (2012) Neurofibromatosis-like phenotype in *Drosophila* caused by lack of glucosylceramide extension. *PNAS* 109: 6987–6992.
40. Coetzee T, Fujita N, Dupree J, Shi R, Blight A, et al. (1996) Myelination in the absence of galactocerebroside and sulfatide: normal structure with abnormal function and regional instability. *Cell* 86: 209–219.
41. Ingrund S, Hartmann D, Farwanah H, Eckhardt M, Sandhoff R, et al. (2009) Adult ceramide synthase 2 (CERS2)-deficient mice exhibit myelin sheath defects, cerebellar degeneration, and hepatocarcinomas. *J Biol Chem* 284: 33549–33560.
42. Sun B, Xu P, Salvaterra PM (1999) Dynamic visualization of nervous system in live *Drosophila*. *Proc Natl Acad Sci U S A* 96: 10438–10443.
43. Sepp KJ, Auld VJ (1999) Conversion of lacZ enhancer trap lines to GAL4 lines using targeted transposition in *Drosophila melanogaster*. *Genetics* 151: 1093–1101.
44. Awasaki T, Lai SL, Ito K, Lee T (2008) Organization and postembryonic development of glial cells in the adult central brain of *Drosophila*. *J Neurosci* 28: 13742–13753.
45. Stewart BA, Atwood HL, Renger JJ, Wang J, Wu CF (1994) Improved stability of *Drosophila* larval neuromuscular preparations in haemolymph-like physiological solutions. *J Comp Physiol A* 175: 179–191.
46. Leiserson WM, Forbush B, Keshishian H (2011) *Drosophila* glia use a conserved cotransporter mechanism to regulate extracellular volume. *Glia* 59: 320–332.
47. Carvalho M, Schwudke D, Sampaio JL, Palm W, Riezman I, et al. (2010) Survival strategies of a sterol auxotroph. *Development* 137: 3675–3685.
48. Herzog R, Schwudke D, Schuhmann K, Sampaio JL, Bornstein SR, et al. (2011) A novel informatics concept for high-throughput shotgun lipidomics based on the molecular fragmentation query language. *Genome Biol* 12: R8.
49. Bainton RJ, Tsai LT, Schwabe T, DeSalvo M, Gaul U, et al. (2005) moody encodes two GPCRs that regulate cocaine behaviors and blood-brain barrier permeability in *Drosophila*. *Cell* 123: 145–156.
50. Schwabe T, Bainton RJ, Fetter RD, Heberlein U, Gaul U (2005) GPCR signaling is required for blood-brain barrier formation in *drosophila*. *Cell* 123: 133–144.